

Azimuthal di-hadron correlations in d+Au and Au+Au collisions at $\sqrt{s_{NN}} = 200$ GeV from STAR

M. M. Aggarwal,³¹ Z. Ahammed,²² A. V. Alakhverdyants,¹⁸ I. Alekseev,¹⁶ J. Alford,¹⁹ B. D. Anderson,¹⁹ D. Arkhipkin,³ G. S. Averichev,¹⁸ J. Balewski,²³ L. S. Barnby,² S. Baumgart,⁵³ D. R. Beavis,³ R. Bellwied,⁵¹ M. J. Betancourt,²³ R. R. Betts,⁸ A. Bhasin,¹⁷ A. K. Bhati,³¹ H. Bichsel,⁵⁰ J. Bielcik,¹⁰ J. Bielcikova,¹¹ B. Biritz,⁶ L. C. Bland,³ B. E. Bonner,³⁷ J. Bouchet,¹⁹ E. Braidot,²⁸ A. V. Brandin,²⁶ A. Bridgeman,¹ E. Bruna,⁵³ S. Bueltmann,³⁰ I. Bunzarov,¹⁸ T. P. Burton,³ X. Z. Cai,⁴¹ H. Caines,⁵³ M. Calderón de la Barca Sánchez,⁵ O. Catu,⁵³ D. Cebra,⁵ R. Cendejas,⁶ M. C. Cervantes,⁴³ Z. Chajecki,²⁹ P. Chaloupka,¹¹ S. Chattopadhyay,⁴⁸ H. F. Chen,³⁹ J. H. Chen,⁴¹ J. Y. Chen,⁵² J. Cheng,⁴⁵ M. Cherney,⁹ A. Chikanian,⁵³ K. E. Choi,³⁵ W. Christie,³ P. Chung,¹¹ R. F. Clarke,⁴³ M. J. M. Coddington,⁴³ R. Corliss,²³ J. G. Cramer,⁵⁰ H. J. Crawford,⁴ D. Das,⁵ S. Dash,¹³ A. Davila Leyva,⁴⁴ L. C. De Silva,⁵¹ R. R. Debebe,³ T. G. Dedovich,¹⁸ A. A. Derevschikov,³³ R. Derradi de Souza,⁷ L. Didenko,³ P. Djawotho,⁴³ S. M. Dogra,¹⁷ X. Dong,²² J. L. Drachenberg,⁴³ J. E. Draper,⁵ J. C. Dunlop,³ M. R. Dutta Mazumdar,⁴⁸ L. G. Efimov,¹⁸ E. Elhalhuli,² M. Elnimr,⁵¹ J. Engelage,⁴ G. Eppley,³⁷ B. Erazmus,⁴² M. Estienne,⁴² L. Eun,³² O. Evdokimov,⁸ P. Fachini,³ R. Fatemi,²⁰ J. Fedorisin,¹⁸ R. G. Fersch,²⁰ P. Filip,¹⁸ E. Finch,⁵³ V. Fine,³ Y. Fisyak,³ C. A. Gagliardi,⁴³ D. R. Gangadharan,⁶ M. S. Ganti,⁴⁸ E. J. Garcia-Solis,⁸ A. Geromitsos,⁴² F. Geurts,³⁷ V. Ghazikhanian,⁶ P. Ghosh,⁴⁸ Y. N. Gorbunov,⁹ A. Gordon,³ O. Grebenyuk,²² D. Grosnick,⁴⁷ S. M. Guertin,⁶ A. Gupta,¹⁷ N. Gupta,¹⁷ W. Guryn,³ B. Haag,⁵ A. Hamed,⁴³ L-X. Han,⁴¹ J. W. Harris,⁵³ J. P. Hays-Wehle,²³ M. Heinz,⁵³ S. Heppelmann,³² A. Hirsch,³⁴ E. Hjort,²² A. M. Hoffman,²³ G. W. Hoffmann,⁴⁴ D. J. Hofman,⁸ M. J. Horner,²² B. Huang,³⁹ H. Z. Huang,⁶ T. J. Humanic,²⁹ L. Huo,⁴³ G. Igo,⁶ P. Jacobs,²² W. W. Jacobs,¹⁵ C. Jena,¹³ F. Jin,⁴¹ C. L. Jones,²³ P. G. Jones,² J. Joseph,¹⁹ E. G. Judd,⁴ S. Kabana,⁴² K. Kajimoto,⁴⁴ K. Kang,⁴⁵ J. Kapitan,¹¹ K. Kauder,⁸ D. Keane,¹⁹ A. Kechechyan,¹⁸ D. Kettler,⁵⁰ D. P. Kikola,²² J. Kiryluk,²² A. Kisiel,⁴⁹ S. R. Klein,²² A. G. Knospe,⁵³ A. Kocoloski,²³ D. D. Koetke,⁴⁷ T. Kollegger,¹² J. Konzer,³⁴ I. Koralt,³⁰ L. Koroleva,¹⁶ W. Korsch,²⁰ L. Kotchenda,²⁶ V. Kouchpil,¹¹ P. Kravtsov,²⁶ K. Krueger,¹ M. Krus,¹⁰ L. Kumar,¹⁹ P. Kurnadi,⁶ M. A. C. Lamont,³ J. M. Landgraf,³ S. LaPointe,⁵¹ J. Lauret,³ A. Lebedev,³ R. Lednicky,¹⁸ C-H. Lee,³⁵ J. H. Lee,³ W. Leight,²³ M. J. LeVine,³ C. Li,³⁹ L. Li,⁴⁴ N. Li,⁵² W. Li,⁴¹ X. Li,⁴⁰ X. Li,³⁴ Y. Li,⁴⁵ Z. M. Li,⁵² G. Lin,⁵³ S. J. Lindenbaum,²⁷ * M. A. Lisa,²⁹ F. Liu,⁵² H. Liu,⁵ J. Liu,³⁷ T. Ljubicic,³ W. J. Llope,³⁷ R. S. Longacre,³ W. A. Love,³ Y. Lu,³⁹ X. Luo,³⁹ G. L. Ma,⁴¹ Y. G. Ma,⁴¹ D. P. Mahapatra,¹³ R. Majka,⁵³ O. I. Mall,⁵ L. K. Mangotra,¹⁷ R. Manweiler,⁴⁷ S. Margetis,¹⁹ C. Markert,⁴⁴ H. Masui,²² H. S. Matis,²² Yu. A. Matulenko,³³ D. McDonald,³⁷ T. S. McShane,⁹ A. Meschanin,³³ R. Milner,²³ N. G. Minaev,³³ S. Mioduszewski,⁴³ A. Mischke,²⁸ M. K. Mitrovski,¹² B. Mohanty,⁴⁸ M. M. Mondal,⁴⁸ B. Morozov,¹⁶ D. A. Morozov,³³ M. G. Munhoz,³⁸ B. K. Nandi,¹⁴ C. Nattrass,⁵³ T. K. Nayak,⁴⁸ J. M. Nelson,² P. K. Netrakanti,³⁴ M. J. Ng,⁴ L. V. Nogach,³³ S. B. Nurushev,³³ G. Odyniec,²² A. Ogawa,³ V. Okorokov,²⁶ E. W. Oldag,⁴⁴ D. Olson,²² M. Pachr,¹⁰ B. S. Page,¹⁵ S. K. Pal,⁴⁸ Y. Pandit,¹⁹ Y. Panebratsev,¹⁸ T. Pawlak,⁴⁹ T. Peitzmann,²⁸ V. Perevoztchikov,³ C. Perkins,⁴ W. Peryt,⁴⁹ S. C. Phatak,¹³ P. Pile,³ M. Planinic,⁵⁴ M. A. Ploskon,²² J. Pluta,⁴⁹ D. Plyku,³⁰ N. Poljak,⁵⁴ A. M. Poskanzer,²² B. V. K. S. Potukuchi,¹⁷ C. B. Powell,²² D. Prindle,⁵⁰ C. Pruneau,⁵¹ N. K. Pruthi,³¹ P. R. Pujahari,¹⁴ J. Putschke,⁵³ R. Raniwala,³⁶ S. Raniwala,³⁶ R. L. Ray,⁴⁴ R. Redwine,²³ R. Reed,⁵ H. G. Ritter,²² J. B. Roberts,³⁷ O. V. Rogachevskiy,¹⁸ J. L. Romero,⁵ A. Rose,²² C. Roy,⁴² L. Ruan,³ R. Sahoo,⁴² S. Sakai,⁶ I. Sakrejda,²² T. Sakuma,²³ S. Salur,⁵ J. Sandweiss,⁵³ E. Sangaline,⁵ J. Schambach,⁴⁴ R. P. Scharenberg,³⁴ N. Schmitz,²⁴ T. R. Schuster,¹² J. Seele,²³ J. Seger,⁹ I. Selyuzhenkov,¹⁵ P. Seyboth,²⁴ E. Shahaliev,¹⁸ M. Shao,³⁹ M. Sharma,⁵¹ S. S. Shi,⁵² E. P. Sichtermann,²² F. Simon,²⁴ R. N. Singaraju,⁴⁸ M. J. Skoby,³⁴ N. Smirnov,⁵³ P. Sorensen,³ J. Sowinski,¹⁵ H. M. Spinka,¹ B. Srivastava,³⁴ T. D. S. Stanislaus,⁴⁷ D. Staszak,⁶ J. R. Stevens,¹⁵ R. Stock,¹² M. Strikhanov,²⁶ B. Stringfellow,³⁴ A. A. P. Suaide,³⁸ M. C. Suarez,⁸ N. L. Subba,¹⁹ M. Sumbera,¹¹ X. M. Sun,²² Y. Sun,³⁹ Z. Sun,²¹ B. Surrow,²³ D. N. Svirida,¹⁶ T. J. M. Symons,²² A. Szanto de Toledo,³⁸ J. Takahashi,⁷ A. H. Tang,³ Z. Tang,³⁹ L. H. Tarini,⁵¹ T. Tarnowsky,²⁵ D. Thein,⁴⁴ J. H. Thomas,²² J. Tian,⁴¹ A. R. Timmins,⁵¹ S. Timoshenko,²⁶ D. Tlusty,¹¹ M. Tokarev,¹⁸ T. A. Trainor,⁵⁰ V. N. Tram,²² S. Trentalange,⁶ R. E. Tribble,⁴³ O. D. Tsai,⁶ J. Ulery,³⁴ T. Ullrich,³ D. G. Underwood,¹ G. Van Buren,³ M. van Leeuwen,²⁸ G. van Nieuwenhuizen,²³ J. A. Vanfossen, Jr.,¹⁹ R. Varma,¹⁴ G. M. S. Vasconcelos,⁷ A. N. Vasiliev,³³ F. Videbaek,³ Y. P. Viyogi,⁴⁸ S. Vokal,¹⁸ S. A. Voloshin,⁵¹ M. Wada,⁴⁴ M. Walker,²³ F. Wang,³⁴ G. Wang,⁶ H. Wang,²⁵ J. S. Wang,²¹ Q. Wang,³⁴ X. L. Wang,³⁹ Y. Wang,⁴⁵ G. Webb,²⁰ J. C. Webb,³ G. D. Westfall,²⁵ C. Whitten Jr.,⁶ H. Wieman,²² S. W. Wissink,¹⁵ R. Witt,⁴⁶ Y. F. Wu,⁵² W. Xie,³⁴ N. Xu,²² Q. H. Xu,⁴⁰ W. Xu,⁶ Y. Xu,³⁹ Z. Xu,³ L. Xue,⁴¹ Y. Yang,²¹ P. Yepes,³⁷ K. Yip,³ I-K. Yoo,³⁵ Q. Yue,⁴⁵ M. Zawisza,⁴⁹ H. Zbroszczyk,⁴⁹

W. Zhan,²¹ J. B. Zhang,⁵² S. Zhang,⁴¹ W. M. Zhang,¹⁹ X. P. Zhang,²² Y. Zhang,²² Z. P. Zhang,³⁹ J. Zhao,⁴¹
 C. Zhong,⁴¹ J. Zhou,³⁷ W. Zhou,⁴⁰ X. Zhu,⁴⁵ Y. H. Zhu,⁴¹ R. Zoukarnееv,¹⁸ and Y. Zoukarnееva¹⁸

(STAR Collaboration)

- ¹Argonne National Laboratory, Argonne, Illinois 60439, USA
²University of Birmingham, Birmingham, United Kingdom
³Brookhaven National Laboratory, Upton, New York 11973, USA
⁴University of California, Berkeley, California 94720, USA
⁵University of California, Davis, California 95616, USA
⁶University of California, Los Angeles, California 90095, USA
⁷Universidade Estadual de Campinas, Sao Paulo, Brazil
⁸University of Illinois at Chicago, Chicago, Illinois 60607, USA
⁹Creighton University, Omaha, Nebraska 68178, USA
¹⁰Czech Technical University in Prague, FNSPE, Prague, 115 19, Czech Republic
¹¹Nuclear Physics Institute AS CR, 250 68 Řež/Prague, Czech Republic
¹²University of Frankfurt, Frankfurt, Germany
¹³Institute of Physics, Bhubaneswar 751005, India
¹⁴Indian Institute of Technology, Mumbai, India
¹⁵Indiana University, Bloomington, Indiana 47408, USA
¹⁶Alikhanov Institute for Theoretical and Experimental Physics, Moscow, Russia
¹⁷University of Jammu, Jammu 180001, India
¹⁸Joint Institute for Nuclear Research, Dubna, 141 980, Russia
¹⁹Kent State University, Kent, Ohio 44242, USA
²⁰University of Kentucky, Lexington, Kentucky, 40506-0055, USA
²¹Institute of Modern Physics, Lanzhou, China
²²Lawrence Berkeley National Laboratory, Berkeley, California 94720, USA
²³Massachusetts Institute of Technology, Cambridge, MA 02139-4307, USA
²⁴Max-Planck-Institut für Physik, Munich, Germany
²⁵Michigan State University, East Lansing, Michigan 48824, USA
²⁶Moscow Engineering Physics Institute, Moscow Russia
²⁷City College of New York, New York City, New York 10031, USA
²⁸NIKHEF and Utrecht University, Amsterdam, The Netherlands
²⁹Ohio State University, Columbus, Ohio 43210, USA
³⁰Old Dominion University, Norfolk, VA, 23529, USA
³¹Panjab University, Chandigarh 160014, India
³²Pennsylvania State University, University Park, Pennsylvania 16802, USA
³³Institute of High Energy Physics, Protvino, Russia
³⁴Purdue University, West Lafayette, Indiana 47907, USA
³⁵Pusan National University, Pusan, Republic of Korea
³⁶University of Rajasthan, Jaipur 302004, India
³⁷Rice University, Houston, Texas 77251, USA
³⁸Universidade de Sao Paulo, Sao Paulo, Brazil
³⁹University of Science & Technology of China, Hefei 230026, China
⁴⁰Shandong University, Jinan, Shandong 250100, China
⁴¹Shanghai Institute of Applied Physics, Shanghai 201800, China
⁴²SUBATECH, Nantes, France
⁴³Texas A&M University, College Station, Texas 77843, USA
⁴⁴University of Texas, Austin, Texas 78712, USA
⁴⁵Tsinghua University, Beijing 100084, China
⁴⁶United States Naval Academy, Annapolis, MD 21402, USA
⁴⁷Valparaiso University, Valparaiso, Indiana 46383, USA
⁴⁸Variable Energy Cyclotron Centre, Kolkata 700064, India
⁴⁹Warsaw University of Technology, Warsaw, Poland
⁵⁰University of Washington, Seattle, Washington 98195, USA
⁵¹Wayne State University, Detroit, Michigan 48201, USA
⁵²Institute of Particle Physics, CCNU (HZNU), Wuhan 430079, China
⁵³Yale University, New Haven, Connecticut 06520, USA
⁵⁴University of Zagreb, Zagreb, HR-10002, Croatia

Yields, correlation shapes, and mean transverse momenta p_T of charged particles associated with intermediate to high- p_T trigger particles ($2.5 < p_T < 10$ GeV/c) in d+Au and Au+Au collisions at $\sqrt{s_{NN}} = 200$ GeV are presented. For associated particles at higher $p_T \gtrsim 2.5$ GeV/c, narrow correlation peaks are seen in d+Au and Au+Au, indicating that the main production mechanism is jet fragmentation. At lower associated particle $p_T < 2$ GeV/c, a large enhancement of the near-

($\Delta\phi \sim 0$) and away-side ($\Delta\phi \sim \pi$) associated yields is found, together with a strong broadening of the away-side azimuthal distributions in Au+Au collisions compared to d+Au measurements, suggesting that other particle production mechanisms play a role. This is further supported by the observed significant softening of the away-side associated particle yield distribution at $\Delta\phi \sim \pi$ in central Au+Au collisions.

PACS numbers: 25.75.Nq, 25.75.Bh

I. INTRODUCTION

The goal of ultra-relativistic heavy-ion collisions is to create a system of deconfined quarks and gluons at high temperature and density and study its properties. In the initial stage of the collision, hard scatterings between partons in the incoming nuclei produce high transverse momentum (p_T) partons that fragment into jets of hadrons with a clear back-to-back di-jet signature [1]. In Au+Au collisions, hard partons traverse the hot and dense colored medium, thus probing the medium through energy loss [2–4].

In-medium jet energy loss was first observed at the Relativistic Heavy Ion Collider (RHIC) as a suppression of hadron spectra at high p_T [5, 6] in Au+Au collisions with respect to p+p collisions. The jet-like structure of hadron production at high p_T was confirmed by measurements of the azimuthal angle difference $\Delta\phi$ distributions of *associated* particles in a certain range of p_T with respect to a *trigger* hadron at a higher p_T [1]. At the highest p_T , a suppression of the away-side yield (around $\Delta\phi \sim \pi$ with respect to the trigger particle) by a factor 3–5 is observed [7]. This suppression is consistent with theoretical calculations that incorporate in-medium energy loss [8, 9]. At lower p_T of the associated particles, a strongly broadened away-side structure is seen in Au+Au collisions, and the associated yields on both the near-side ($\Delta\phi \sim 0$) and away-side ($\Delta\phi \sim \pi$) are enhanced [10, 11]. A number of possible explanations of the away-side broadening at intermediate p_T have been put forward, ranging from fragmentation products of radiated gluons [12, 13] to medium response and the possibility of a Mach-cone shock wave [14–17].

The p_T^{trig} range used in previous studies [10, 11] is the region where the p/ π ratio is large. The large baryon/meson ratio has been interpreted as being due to coalescence/recombination of quarks, which could also have an impact on the jet-like correlation yields, especially for trigger particles in the p_T range 2.0 to 4.0 GeV/ c where coalescence/recombination products [18–20] may be present.

In this paper, we present a systematic exploration of the azimuthal di-hadron correlation shapes and yields with centrality and p_T of the trigger (p_T^{trig}) and associated hadrons (p_T^{assoc}), to investigate the change from broadened correlation peaks with enhanced yields at low

p_T to suppressed away-side yields at high p_T . The analysis is performed on the large statistics sample of Au+Au collisions at $\sqrt{s_{NN}} = 200$ GeV collected by the STAR experiment in the RHIC run in 2004. The d+Au data sample from the year 2003 is used as a reference where no hot and dense matter is formed, because the minimum bias p+p data collected by STAR has limited statistics. Earlier studies have shown that di-hadron correlations in p+p and d+Au collisions are similar [1].

II. EXPERIMENTAL SETUP AND DATA SETS

The measurements presented in this paper were performed with the STAR detector at RHIC [21]. Charged tracks are reconstructed with the Time Projection Chamber (TPC) [22].

For Au+Au collisions, two different online event selections (triggers), minimum bias and central, were used. The central trigger selection was based on the energy deposited in the two Zero-Degree Calorimeters (ZDCs) which measure spectator fragments and small-angle particle production [21]. The trigger selected the most central 12% of the total hadronic cross section, based on a maximum energy deposited in the ZDCs and a minimum multiplicity in the Central Trigger Barrel (CTB) [23]. The central trigger also uses time information from the Beam-Beam Counters (BBC) to restrict the primary vertex position z_{vtx} to be within approximately ± 30 cm of the center of the detector along the beam direction. The minimum bias (MB) trigger is based on a ZDC coincidence (a threshold amount of energy in each ZDC) and required a minimum multiplicity in the CTB to reject non-hadronic interactions. For the minimum bias sample, events were selected to have $|z_{vtx}| < 25$ cm. A total of 21M minimum bias events and 18M central triggered Au+Au events were used.

For d+Au collisions, the minimum bias trigger was defined by requiring that at least one beam-rapidity neutron impinge on the ZDC in the Au beam direction. The measured minimum bias cross section amounts to $95 \pm 3\%$ of the total d+Au geometric cross section [1]. For d+Au events, the distribution of primary vertices along the beamline was wider than during the Au+Au run. The events were selected to be within ± 50 cm from the center of the detector along the beam line. A total of 3.4M d+Au events were selected for this analysis.

The Au+Au events are further divided into centrality classes based on the uncorrected charged particle multiplicity in the range $|\eta| < 0.5$ as measured by the TPC. We

*Deceased

present results for the following centrality ranges: 0-12% (from the central triggered data set), 20-40%, 40-60%, and 60-80% (from the MB data set) of the total hadronic cross section, with 0% referring to the most central collisions.

III. DATA ANALYSIS

Di-hadron correlations are constructed using charged particles measured in the TPC. All particles are selected to have pseudo-rapidity in the range $-1.0 < \eta < 1.0$, so that they fall well within the TPC acceptance. To reject background tracks at high p_T , tracks were required to have at least 20 measured points in the TPC (out of 45) and a distance of closest approach (dca) to the event vertex of less than 1 cm to reduce the contribution from secondary particles.

The results are corrected for single particle acceptance and detection efficiency as well as for the pair acceptance as a function of $\Delta\phi$. The single particle reconstruction efficiency as a function of η , p_T , and centrality is determined using hits from a Monte Carlo simulation which are embedded into real data events. The tracking efficiency depends sensitively on the gain in the proportional readout chamber of the TPC and thus on the atmospheric pressure. Uncertainties in details of these effects give rise to an overall 5% systematic uncertainty in the absolute yields given in this paper. In most cases, the uncertainty from the background subtraction as described in the next section is larger than the systematic uncertainty from the tracking efficiency. The TPC sector boundaries introduce a dependence of the pair acceptance on angle difference $\Delta\phi$, which was determined from mixed events. No $\Delta\eta$ pair acceptance correction has been applied. A small inefficiency due to tracks crossing inside the TPC volume affects the associated hadron distribution at small pair separation in $(\Delta\eta, \Delta\phi)$. This effect manifests itself as a reduced efficiency for small but finite $\Delta\phi$, at positive or negative $\Delta\phi$, depending on the sign of the curvature of the associate track. A correction was performed by first curvature-sorting the distributions and then reflecting a few bins from the unaffected area to the area where the inefficiency occurs, thus restoring the symmetry between positive and negative $\Delta\phi$.

Figure 1 shows an example azimuthal angle difference distribution for trigger particles with $4.0 < p_T^{trig} < 6.0$ GeV/c and associated particles with $1.0 < p_T^{assoc} < 2.5$ GeV/c in 0-12% central Au+Au collisions. The distribution is divided by the number of trigger hadrons to give the associated yield per trigger hadron. The associated hadron distribution contains a background of uncorrelated particles which has a $\cos(2\Delta\phi)$ modulation due to the correlation of all particles with the reaction plane through elliptic flow, v_2 . We model the background using the function $B(1 + 2\langle v_2^{trig} \rangle \langle v_2^{assoc} \rangle \cos(2\Delta\phi))$, where the v_2 values are from separate flow measurements [24]. The function is normalized to the data in the region

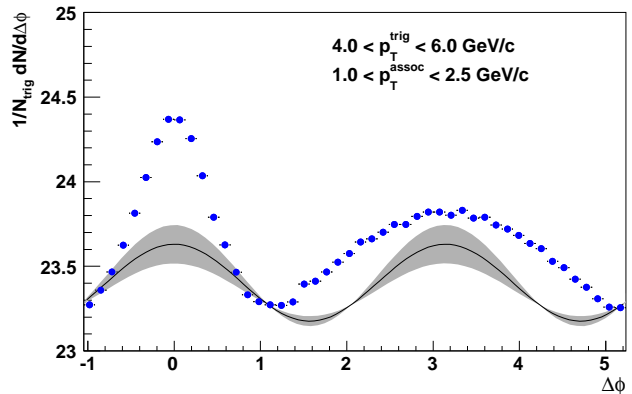


FIG. 1: (Color online) Azimuthal distribution of associated charged particles with $1.0 < p_T^{assoc} < 2.5$ GeV/c with respect to trigger particles with $4.0 < p_T^{trig} < 6.0$ GeV/c in 0-12% central Au+Au collisions. The curve shows the modulation of the background due to elliptic flow v_2 and the grey band indicates the uncertainty on the elliptic flow of the background (see text).

$0.8 < |\Delta\phi| < 1.2$, where the signal is apparently small, and then subtracted. This background normalisation procedure is often referred to as the ZYA1 ('Zero Yield at 1 radian') or ZYAM ('Zero Yield At Minimum') method [25].

The method of normalising the combinatorial background level in the region around $|\Delta\phi| = 1$ has first been used for di-hadron correlations at higher momenta [7, 10], where there are narrow peaks on the near- and away-side, separated by a largely 'signal-free' region. At lower p_T , the correlation peaks are broader, and there is no clear signal-free region, so that the background normalisation is more ambiguous. In addition, due to the larger combinatorial background, the elliptic flow modulation of the background is of similar size as the trigger-associated-hadron correlation signal. The ZYA1 method provides a simple prescription to separate signal and background, which we will use throughout the paper. An alternative approach would be to decompose the correlation shape using a fit function with components representing the flow modulation of the background and the assumed shapes of near- and away-side correlation peaks [26, 27]. The unsubtracted azimuthal hadron distributions are provided in the Appendix and can be used for such a procedure.

The nominal v_2 value used for the subtraction is the mean of the v_2 measured using the reaction plane method with the Forward TPC and the four-particle cumulant method, which have different sensitivity to non-flow effects and flow fluctuations [24] (line in Fig. 1). The difference between the two results is used as the estimate of the systematic uncertainty in v_2 and this range is shown by the band in Fig. 1. For the d+Au results a constant pedestal (normalized in the same $\Delta\phi$ range) was subtracted.

IV. RESULTS

A. Azimuthal di-hadron distributions

Fig. 2 shows the background subtracted associated hadron $\Delta\phi$ distributions with $1.0 < p_T^{assoc} < 2.5$ GeV/c for 4 centrality selections, 60-80%, 40-60%, 20-40% and 0-12%, and 4 trigger selections, $2.5 < p_T^{trig} < 3.0$ GeV/c, $3.0 < p_T^{trig} < 4.0$ GeV/c, $4.0 < p_T^{trig} < 6.0$ GeV/c, and $6.0 < p_T^{trig} < 10.0$ GeV/c. Results are presented for two different ranges in the pseudo-rapidity difference between the trigger and associated particles $|\Delta\eta|$. The shapes are very similar for both $\Delta\eta$ selections in all panels (there is an overall reduction in the away-side yields due to the smaller acceptance for $|\Delta\eta| < 0.7$). For reference, the di-hadron distributions without background subtraction are shown in the Appendix, where also the v_2 values and background normalization values (B) used to subtract the background are given. The systematic uncertainties on the v_2 values for the background are shown by the bands around the data points. The d+Au results (open circles) are also shown for reference.

In Fig. 2, top row, one observes that the jet-like correlations in peripheral (60-80% centrality) Au+Au collisions are very similar to the d+Au result, indicating that such correlations in peripheral Au+Au collisions can be described as a superposition of independent p+p collisions. The near- and away-side yields of associated particles increase with p_T^{trig} , as expected from parton fragmentation.

For more central events, a significant increase of both the near- and the away-side yields is seen in Au+Au collisions relative to d+Au. The relative increase of the near-side yield is larger for lower p_T^{trig} (top row) than for higher p_T^{trig} . For peripheral events, the near-side results for $|\Delta\eta| < 0.7$ do not differ significantly from the full acceptance results, demonstrating that the correlated yield is at relatively small $\Delta\eta$, as expected from jet fragmentation. For more central collisions, on the other hand, a significant fraction of the associated yield is at large $|\Delta\eta| > 0.7$ for the lower p_T^{trig} , indicating a significant long-range correlation in $\Delta\eta$, possibly due to an interplay between the soft bulk dynamics of longitudinal flow and jet-like di-hadron structure [28]. It has also been argued recently that this long-range correlation in $\Delta\eta$ could be caused by long-range structures in the medium, due to density fluctuations in the medium [29] or color flux tubes [30–32]. The ‘ridge’-like correlation structure in $\Delta\eta$ is further explored in other STAR publications [26, 33?, 34].

It is interesting to note that the largest relative enhancement of the near-side yield is observed for the lower p_T^{trig} , 2.5 – 4.0 GeV/c. It has been suggested that particle production in this momentum range has a large contribution from coalescence of quarks from bulk partonic matter [18–20]. This production mechanism would not lead to jet-like structures. Trigger hadrons formed by this mechanism would increase the number of trigger hadrons,

without increasing the associated yield, leading to a reduced per-trigger associated yield, in contrast to what is observed in Fig. 2. The increased associated yield at intermediate p_T indicates that if coalescence is a significant source of hadron production at intermediate p_T , it has to generate angular correlation structure, either through shower-thermal coalescence [35] or local fluctuations in the medium density or temperature, e.g. due to heating of the medium by the passage of a parton [36]. So far, most calculations of such effects are qualitative at best. Quantitative predictions for these processes should be made and compared to the data. Measurements with identified baryons and mesons as trigger and associated particles [37, 38] can be used to explore the possible contributions from coalescence.

The away-side yield of associated particles at low p_T^{trig} (top row Fig. 2) evolves significantly in both shape and yield with centrality: the shape becomes much broader than the d+Au reference and the yield increases. For 20-40% central collisions the distribution becomes flat or slightly double-peaked, with a shallow minimum at $\Delta\phi = \pi$. In the most central collisions the distribution is double-peaked for the lowest p_T^{trig} . With increasing p_T^{trig} , the away-side shape becomes flatter. Overall, there is a smooth evolution of the peak shape with centrality and p_T^{trig} . The value of p_T^{trig} for which the away-side becomes flat or double-peaked decreases with centrality. Note that the double-peak shape is not seen in the raw signal in Fig. 1 and only appears after the subtraction of the v_2 -modulated background. In that sense, the double-peak structure is generated by imposing a separation between flow and non-flow in the analysis of azimuthal correlations. This separation is not unambiguous and remains under active investigation.

For the most central collisions, the broadening of the away-side structure is so large that the near- and away-side peaks may overlap, making it impossible to unambiguously distinguish the correlation structure from the background without other inputs. For the present analysis, we have chosen to use the same background normalization procedure for all centrality bins and p_T bins, *i.e.* to normalize the v_2 -modulated background to the signal in the range $0.8 < |\Delta\phi| < 1.2$ and subtract it.

In Fig. 3 we focus on central data where the largest modifications of the correlation shapes and yields are found. The figure shows the correlation shapes in the 0-12% central event sample for different selections of p_T^{assoc} and p_T^{trig} . As in Fig. 2, results are given for the full $\Delta\eta$ -acceptance (solid circles) as well as a restricted range $|\Delta\eta| < 0.7$ (squares), and for d+Au collisions (open circles). The distributions before background subtractions and the background normalization and v_2 values are given in the Appendix.

On the near-side, we observe again a large increase of the yield in central Au+Au collisions compared to d+Au collisions. The yield depends on the $\Delta\eta$ -selection used, indicating that there is significant associated yield at $\Delta\eta > 0.7$. The relative size of the enhancement de-

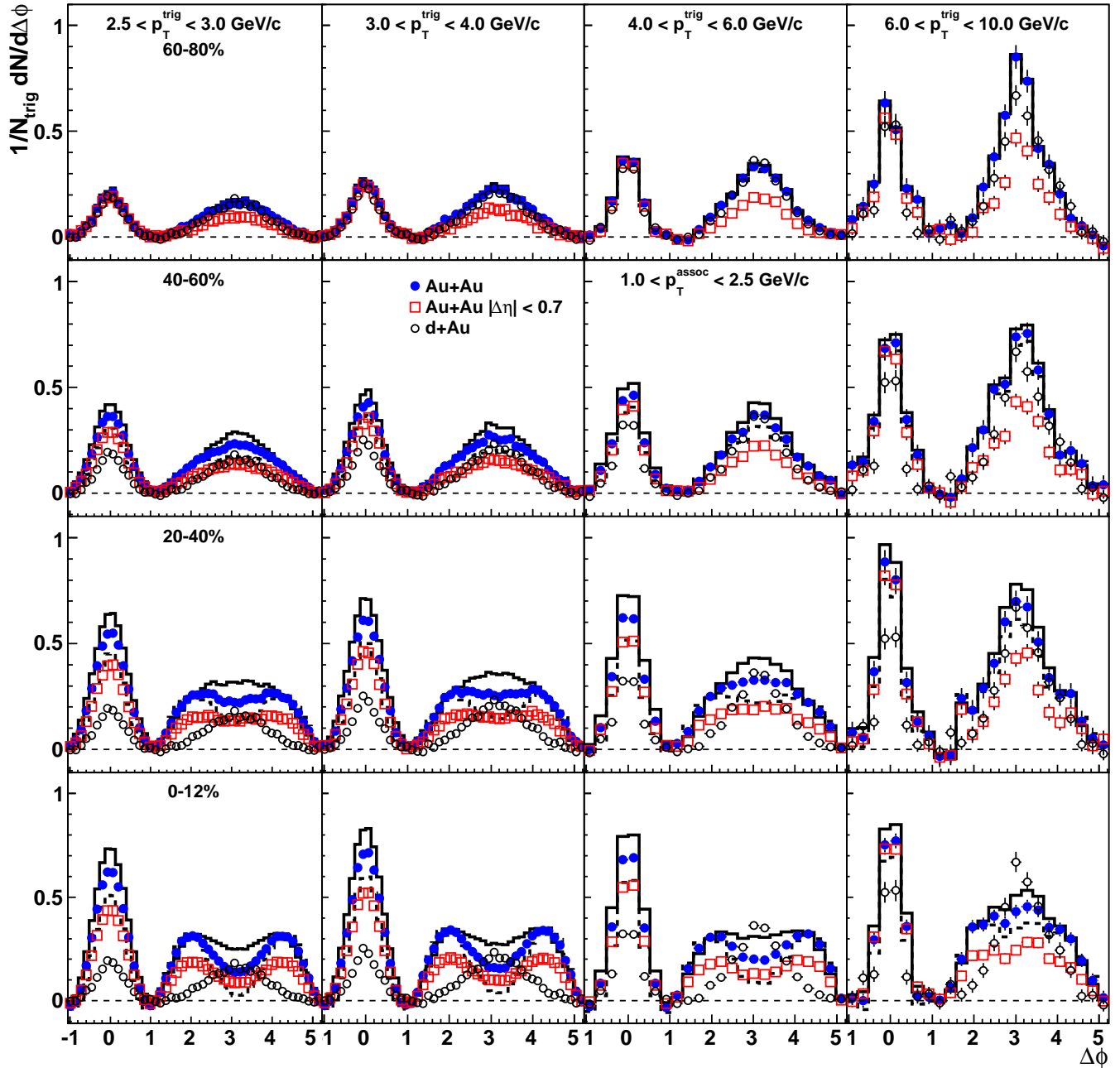


FIG. 2: (Color online) Background-subtracted azimuthal angle difference distributions for associated particles with p_T between 1.0 and 2.5 GeV/c and for different ranges of trigger particle p_T , ranging from 2.5 – 3.0 GeV/c (left column) to 6 – 10 GeV/c (right column). Results are shown for Au+Au collisions (solid circles) with different centrality (rows) and d+Au reference results (open circles). The rapidity range is $|\eta| < 1$ and as a result the rapidity-difference $|\Delta\eta| < 2$. Open red squares show results for a restricted acceptance of $|\Delta\eta| < 0.7$, using tracks within $|\eta| < 1$. The solid and dashed histograms show the upper and lower range of the systematic uncertainty due to the v_2 modulation of the subtracted background.

depends on p_T^{assoc} and p_T^{trig} . The measured jet-like yield in d+Au collisions increases faster with p_T^{trig} (going from left to right in Fig. 3) than in Au+Au collisions, reducing the relative size of the enhancement in Au+Au. The associated yield decreases with increasing p_T^{assoc} for both d+Au and Au+Au collisions, but the decrease is stronger in Au+Au, so that the measured yields in Au+Au ap-

proach the d+Au results at the highest p_T^{assoc} . A summary of the yields is presented in Fig. 6 (Section IV C).

On the away-side, we observe a broadening and enhancement of the yield in Au+Au compared to d+Au, except at $2.5 < p_T^{assoc} < 4.0$ GeV/c (bottom row of Fig. 3), where a broadening is seen, while the yield is smaller than in d+Au. For $6 < p_T^{trig} < 10$ GeV/c (right-

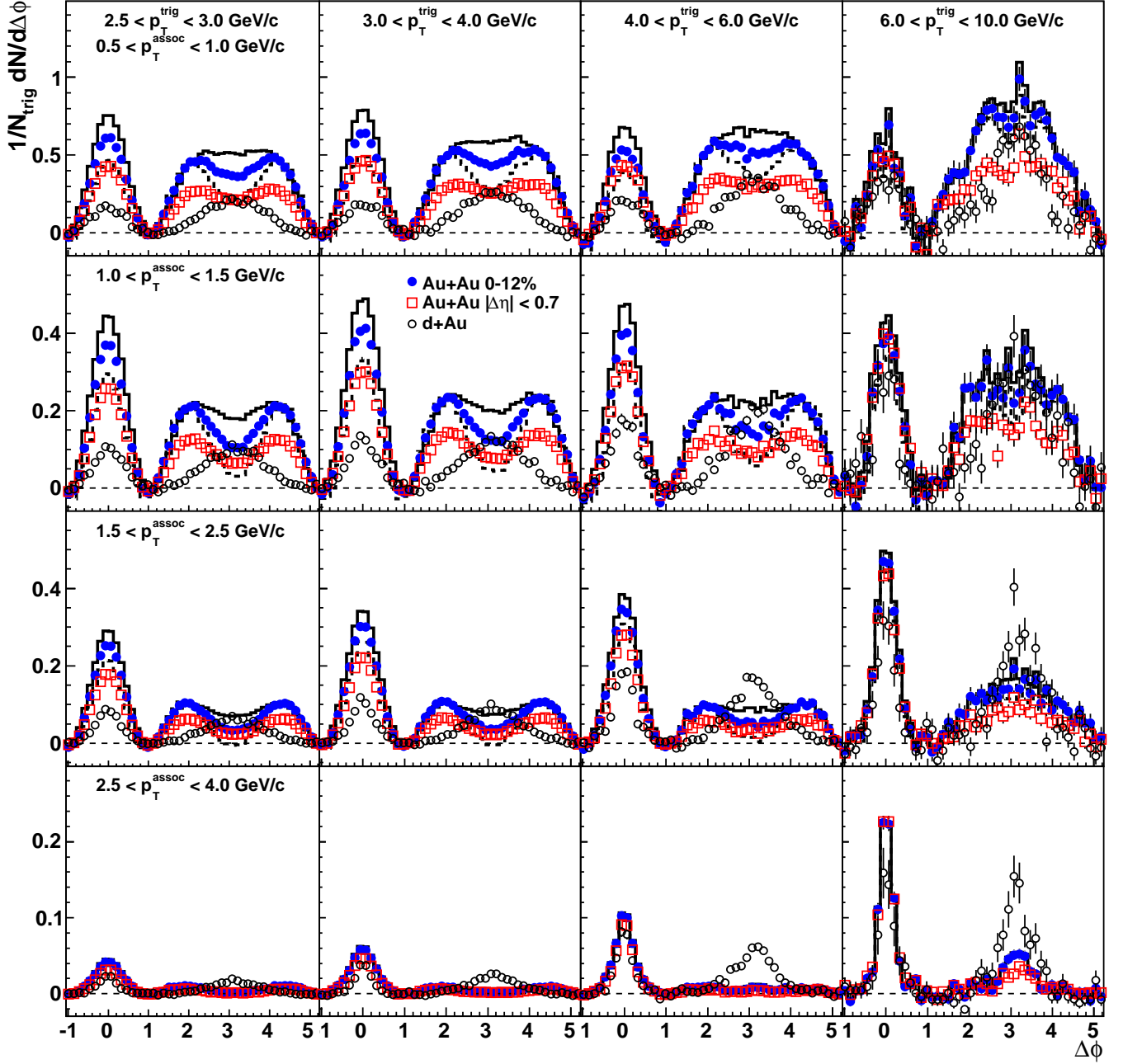


FIG. 3: (Color online) Background-subtracted azimuthal angle difference distributions for different p_T^{trig} (columns) and p_T^{assoc} (rows) in 0-12% central Au+Au collisions (solid circles) and d+Au reference results (open circles). The rapidity range is $|\eta| < 1$ and as a result the rapidity-difference $|\Delta\eta| < 2$. Open red squares show results for a restricted acceptance of $|\Delta\eta| < 0.7$, using tracks with $|\eta| < 1$. The solid and dashed histograms show the upper and lower range of the systematic uncertainty due to the v_2 modulation of the subtracted background.

most column in Fig. 3), a narrow peak appears at large p_T^{assoc} in Au+Au, similar to what is seen in d+Au collisions and at higher p_T in Au+Au collisions [7].

Although the shape of the away-side distribution changes with p_T^{trig} and p_T^{assoc} , there seems to be no gradual broadening as a function of p_T : the rising flanks of the away-side distribution are at similar $\Delta\phi$ in the entire range $0.5 < p_T^{assoc} < 2.5$ GeV/c and $2.5 < p_T^{trig} < 6$. In

fact, it could be argued that the away-side distribution is as broad as possible; there is no $\Delta\phi$ region without correlation signal.

The broad away-side correlation structure in Au+Au collisions is a truly remarkable observation. Although some broadening of the away-side correlation in Au+Au collisions would be expected due to increased acoplanarity (k_T) due to multiple scattering of the parton in

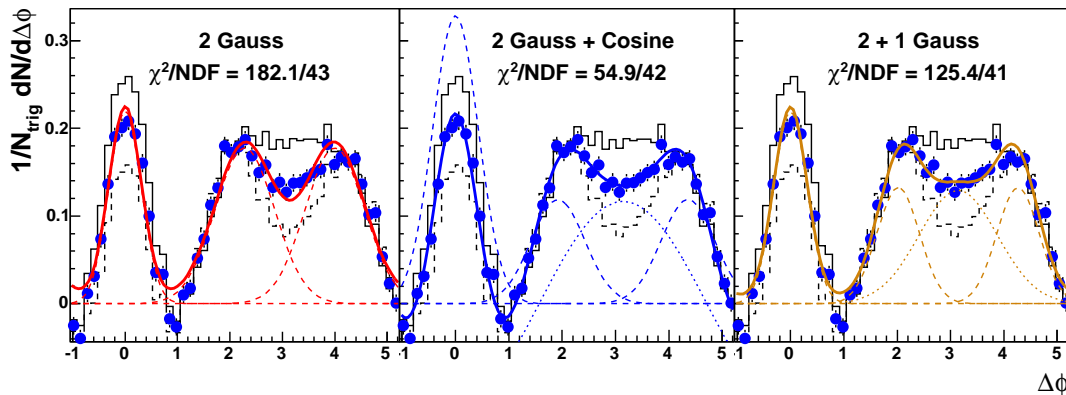


FIG. 4: (Color online) Background-subtracted associated hadron distribution in 0-12% central Au+Au collisions with $0.8 < p_T^{assoc} < 1.0$ GeV/c and $4 < p_T^{trig} < 6$ GeV/c. The colored curves indicate fits with 3 different functional forms for the away-side shape: (left panel) symmetric identical Gaussian distributions (2 Gauss), (middle panel) adding a $\cos\Delta\phi$ background distribution (2 Gauss + Cosine), and (right panel) adding a third Gaussian as the away-side jet-like component (2+1 Gauss). The histograms indicate the uncertainty on the background shape due to elliptic flow.

the medium, the structures seen in Fig. 3 are broader than would be expected from such a mechanism [12]. It has, however, been pointed out that kinematic selection effects on in-medium gluon radiation may lead to a non-trivial structure in the angular distributions [13]. It has also been argued that a fast parton may generate sound waves in the bulk quark-gluon matter which would lead to a Mach-cone shock wave [14–17]. Evidence for a conical emission pattern has been found in three-particle correlation measurements [39]. The broad structure seen in the di-hadron distribution could then be the projection of the conical pattern on $\Delta\phi$. Another mechanism that may produce conical emission from a fast parton is QCD Cherenkov radiation [40, 41]. There are two other calculations that show a broad, double-peaked away-side structure without implementing a specific mechanism for conical emission: one is a 3D hydrodynamical calculation which includes local density fluctuations in the initial state [29] and the other is the AMPT model [42]. It is worth noting that in the 3D hydrodynamical model, there is also no explicit introduction of hard partons or jets; the correlation arises purely from the medium. All these models should be confronted with the data presented in Figs 2 and 3 as well as the three-particle correlation data in [39].

In addition to the change of the correlation shapes, a significant increase of the yields is seen in Au+Au collisions relative to d+Au collisions, for most of the p_T -selections in Fig. 3, both on the near- and the away-side. The yield increase implies that trigger hadrons in Au+Au collisions are accompanied by a larger energy flow than trigger hadrons with the same transverse momentum in elementary collisions. This would be compatible with a scenario where the leading hadron is softened due to energy loss so that trigger hadrons in Au+Au collisions select a larger initial parton energy than in d+Au or p+p collisions.

B. Away-side shapes

To further characterize the broad shape of the away-side associated hadron distributions in Figs 2 and 3, the data were fitted with different parameterizations. Three different functional forms were used, all of which are based on the assumption that there is significant yield in a cone in $(\Delta\eta, \Delta\phi)$ around the away-side parton. The projection of this cone on $\Delta\phi$ would give rise to two peaks symmetric around $\Delta\phi = \pi$. Fig. 4 shows the associated hadron distribution after background subtraction for $4 < p_T^{trig} < 6$ GeV/c and $0.8 < p_T^{assoc} < 1.0$ GeV/c fitted with three different functional forms that include two Gaussian distributions at $\Delta\phi = \pi \pm \Delta$ on the away-side. The left panel of Fig. 4 shows the simplest ansatz, using just two Gaussian peaks on the away side and a single Gaussian peak on the near side. To account for correlations induced by momentum conservation or remnant jet structure, we add a $\cos(\Delta\phi)$ distribution (middle panel of Fig. 4) or a third Gaussian peak (with a different width and amplitude) at $\Delta\phi = \pi$ (right panel Fig. 4). The three parameterizations are referred to as 2 Gauss, 2 Gauss + Cosine and 2+1 Gauss, respectively. The best fit is obtained when using the 2 Gauss + Cosine function, as can be seen from the χ^2 values given in the figure.

Figure 5 shows Δ , the angle (in radians) between the Gaussian peaks and $\Delta\phi = \pi$, as a function of p_T^{assoc} , for the three different parameterizations of the away-side shape for $4 < p_T^{trig} < 6$ GeV/c in the 0-12% most central collisions. Similar results were obtained for $3 < p_T^{trig} < 4$ GeV/c (not shown).

The peak positions Δ in Fig. 5 show a slow increase with p_T^{assoc} for the fits with the Symmetric Gaussian form. This functional form alone however, does not provide a good description of the away-side shape for larger p_T^{trig} and p_T^{assoc} . When an away-side contribution at

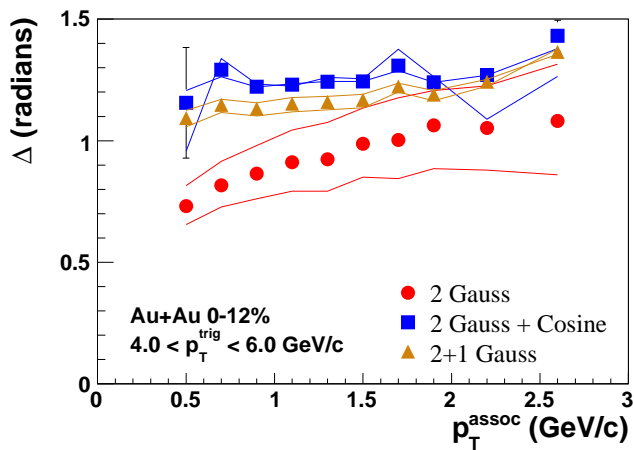


FIG. 5: (Color online) The angle Δ between the away-side peaks and $\Delta\phi = \pi$ for $4 < p_T^{trig} < 6$ GeV/c in 0-12% central Au+Au collisions as a function of p_T^{assoc} . Three different parametrisations of the away-side peak shape were used (see text). The lines show the systematic uncertainty from v_2 variation while the errors are statistical errors from the fit.

$\Delta\phi = \pi$ is included (2+1 Gauss and 2 Gauss+Cosine shapes), the peak position Δ is close to 1.2 and approximately independent of p_T^{assoc} . This observation is qualitatively consistent with predictions for a Mach Cone developing in the hot and dense medium of the early stage of the collision [15] and with existing results on three-particle azimuthal correlations [39].

C. Associated particle spectra

Figure 6 shows the integrated yield in the near-side peak ($|\Delta\phi| < 0.9$) and away-side ($|\Delta\phi| > 0.9$) as a function of p_T^{assoc} in central Au+Au collisions and d+Au collisions for four p_T^{trig} intervals. The lower panels of the figures show the ratio of the associated yields in central Au+Au collisions and d+Au collisions.

For d+Au collisions, the associated yield clearly increases with increasing p_T^{trig} and the slope decreases with p_T^{trig} . These trends are expected from parton fragmentation, where the larger p_T^{trig} selects larger underlying parton energies, thus increasing the multiplicity in the jet and leading to a harder fragmentation.

The lower panels of Fig. 6 show that the ratio of the yields in Au+Au and d+Au is decreasing with p_T^{assoc} , indicating that the fragmentation is softened due to in-medium energy loss. A softer fragmentation also implies that a trigger particle of given momentum selects different parton energies in Au+Au collisions than in d+Au collisions, which could explain some of the enhancement of associated yield at lower p_T^{assoc} in Au+Au collisions. However, it should be noted that a large part of the increased yield at lower p_T^{assoc} is at large $\Delta\eta$, associated with the ridge effect, and is therefore not necessarily from

jet fragments [34]. It is also possible that other sources of particle production, such as parton coalescence and resonance decays, contribute at lower p_T^{trig} and may lead to different behaviour in d+Au and Au+Au.

D. Azimuthal angle dependent mean- p_T

To further characterize the p_T -dependence of associated particle production, we perform an analysis of the inclusive mean- p_T , $\langle p_T \rangle$, of associated particles as a function of $\Delta\phi$. The azimuthal distribution $\langle p_T \rangle(\Delta\phi)$ is calculated by taking the ratio of the p_T -sum distribution $P_T(\Delta\phi)$ and the number distribution $N(\Delta\phi)$

$$\langle p_T \rangle(\Delta\phi) = P_T(\Delta\phi)/N(\Delta\phi). \quad (1)$$

The number distribution $N(\Delta\phi) = 1/N_{trig} dN/d\Delta\phi$, as shown in Fig. 1, while the p_T -sum distribution $P_T(\Delta\phi)$ is formed using the same procedure, but adding the (scalar) transverse momenta as weights in the azimuthal distribution.

To illustrate this method, Fig. 7 shows the inclusive distribution $\langle p_T \rangle(\Delta\phi)$ for $0.25 < p_T^{assoc} < 4.0$ GeV/c and three different p_T^{trig} selections for 0-12% central collisions. On the near-side, a clear increase of $\langle p_T \rangle$ with p_T^{trig} is visible, while the away-side $\langle p_T \rangle$ distributions show a smaller dependence on p_T^{trig} . The lines in Fig. 7 show the background. The elliptic flow of the background is calculated as a weighted average of $v_2^{trig} v_2^{assoc}$. The difference between the p_T -weighted average $\langle v_2 \rangle_{p_T}$, which is used to subtract the background in the p_T -weighted distribution, and the number-weighted $\langle v_2 \rangle_N$, gives rise to the flow modulation of the background shown in the figure.

To calculate the $\langle p_T \rangle$ of associated hadrons, the uncorrelated background is subtracted from both the p_T -weighted and number-weighted distributions before taking the ratio:

$$\langle p_T \rangle(\Delta\phi) = \frac{P_T(\Delta\phi) - B_{p_T}(1 + 2\langle v_2 \rangle_{p_T} \cos(\Delta\phi))}{N(\Delta\phi) - B_N(1 + 2\langle v_2 \rangle_N \cos(\Delta\phi))}, \quad (2)$$

where $N(\Delta\phi)$ and $P_T(\Delta\phi)$ are the same number-weighted and sum- p_T distributions used in Eq. 1, the average $\langle v_2 \rangle$ are defined above and B_{p_T} and B_N are background normalizations which are determined using the ZYAM method separately for the number and sum- p_T distributions.

Figure 8 shows the resulting $\langle p_T \rangle$ of associated hadrons as a function of $\Delta\phi$ in the away-side region for different centrality selections. In the peripheral bins a peaked structure in $\langle p_T \rangle$ is found, similar to the results in d+Au collisions (open circles). With increasing centrality, the $\langle p_T \rangle$ around $\Delta\phi = \pi$ becomes lower. For the most central bin, the results show a minimum at $\Delta\phi = \pi$ for the two softer trigger selections. For the highest trigger selection $6 < p_T^{trig} < 10$ GeV/c, a similar shape is seen, but there may be a slight enhancement at $\Delta\phi = \pi$ even in the most central collisions.

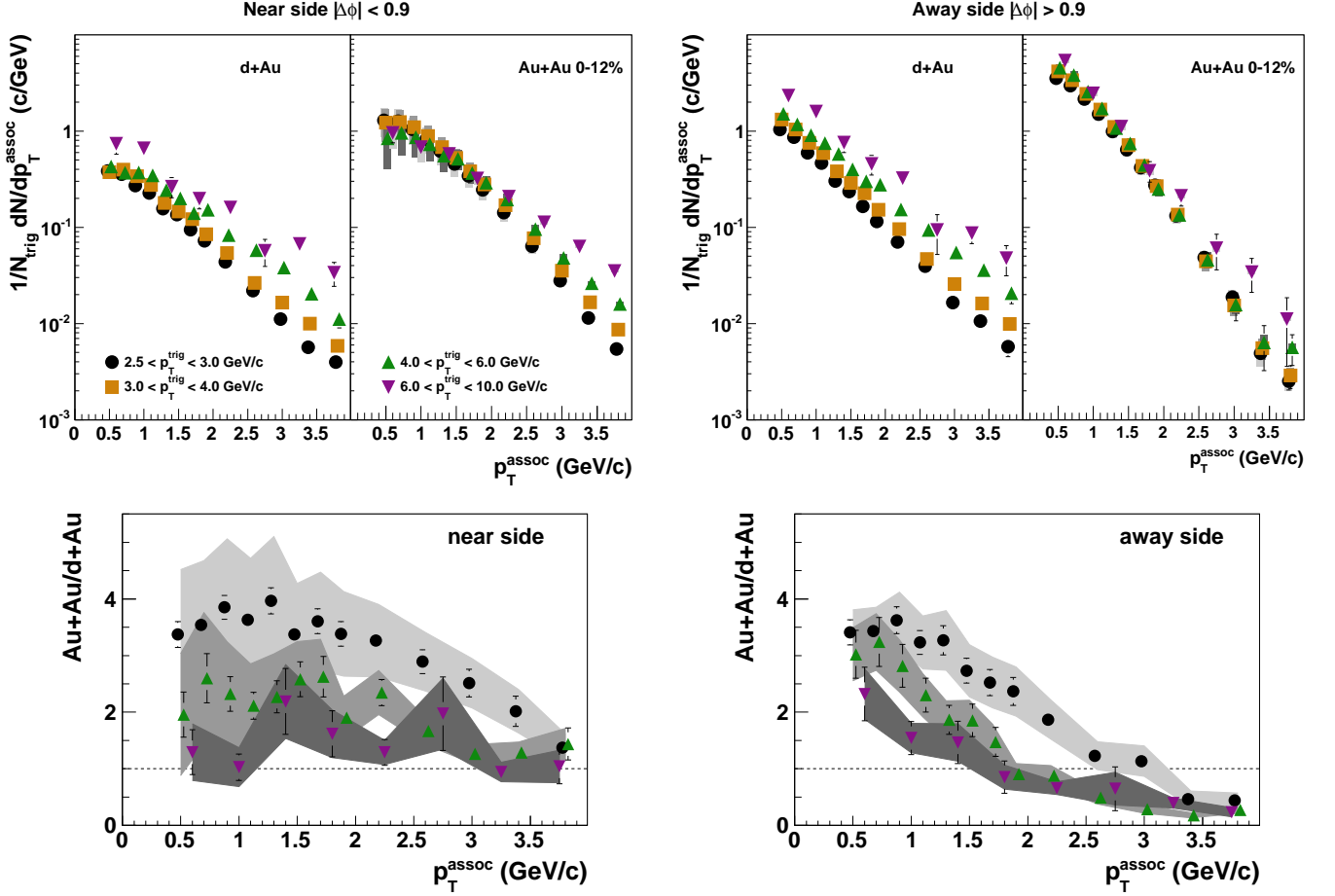


FIG. 6: (Color online) Near-side ($|\Delta\phi| < 0.9$, left panels) and away-side ($|\Delta\phi| > 0.9$, right panels) associated yield per trigger particle for various p_T^{trig} selections as a function of p_T^{assoc} . Results are shown for 0-12% central Au+Au collisions and for d+Au collisions. The bottom panels show the ratios of the per-trigger associated yields in central Au+Au and d+Au collisions. The error bars on the points indicate the statistical uncertainty, including the statistical uncertainty on the subtracted background level. The gray bands indicate the uncertainty from the elliptic flow modulation of the background.

We further study the difference between $\langle p_T \rangle$ in the range $|\Delta\phi - \pi| < \frac{\pi}{6}$ (referred to as “core” in the following) and at $\frac{\pi}{6} < |\Delta\phi - \pi| < \frac{\pi}{2}$ (referred to as “cone” in the following). Figure 9 shows $\langle p_T \rangle$ in these two angular ranges as a function of the collision centrality for two different trigger p_T ranges. The $\langle p_T \rangle$ decreases with centrality approaching the inclusive $\langle p_T \rangle$, a feature already reported in [10] for associated hadrons in the entire away-side region ($|\Delta\phi - \pi| < 2.14$). This reduction of $\langle p_T \rangle$ is likely due to interactions with the medium. The fact that $\langle p_T \rangle$ approaches the $\langle p_T \rangle$ for inclusive particle production in events with a trigger hadron (solid lines in Fig. 9) may indicate that the associated particles at low p_T approach thermalisation with the medium. It is also clear that the $\langle p_T \rangle$ of the core decreases more rapidly than that of the cone hadrons, which suggests that there is significant transport of associated hadrons away from $\Delta\phi = \pi$ due to jet-medium interactions.

V. DISCUSSION AND CONCLUSIONS

In this paper, a comprehensive study of centrality and p_T -dependence of azimuthal di-hadron correlations in Au+Au events is presented. We observe several striking modifications of the correlation structure in Au+Au compared to a d+Au reference. Associated yields on the near- and away-side are enhanced at lower p_T . On the near-side, the increase in yield is partly located at large pseudo-rapidity difference $\Delta\eta$ (see [34] for a more detailed study) and the yields approach the measurement in d+Au collisions at the highest p_T^{trig} . On the away-side, the associated hadron distribution is significantly broadened; in fact, it is broad enough that it is impossible to unambiguously separate jet-like yields from the underlying event. At higher p_T , $p_T^{\text{assoc}} > 2$ GeV/c and $p_T^{\text{trig}} > 6$ GeV/c, the away-side shape is narrow, like in d+Au events. A large enhancement of the away-side yield at low p_T is found, while at higher p_T a suppression is seen with respect to d+Au collisions.

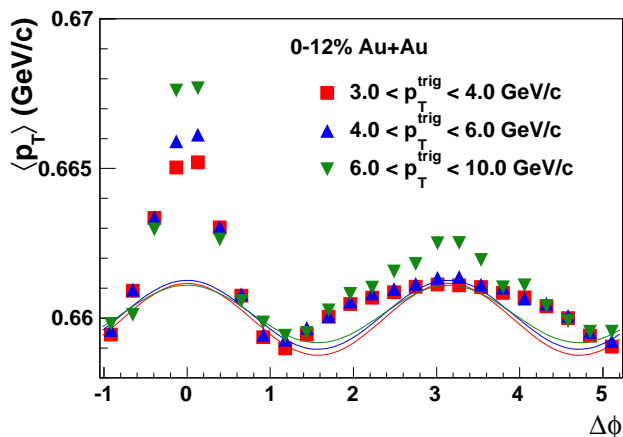


FIG. 7: (Color online) Inclusive, azimuthal $\langle p_T \rangle$ of associated hadrons between 0.25 and 4.0 GeV/c in all events containing various classes of trigger particles. The lines show the v_2 -modulated background for the different trigger ranges, with the colors corresponding to the data points.

These results are qualitatively consistent with a softening of jet fragmentation by in-medium energy loss, leading to an increase of the underlying parton energy selected by a trigger particle at given p_T^{trig} . Some of the changes in the correlation shapes could then be due to fragmentation of radiated gluons.

The strong broadening of the away-side shapes, however, does not seem to fit naturally in a description of particle production from medium modified jet fragmentation. Several alternative mechanisms have been proposed that could give rise to these structures. These can be divided into two categories: collective and radiative phenomena.

Radiative treatments [12, 13, 40, 41, 43] focus on the angular distribution of gluons radiated by the parton propagating through the medium. A large opening angle between the parent parton and radiated gluons is expected when kinematic constraints are imposed. Two simplified calculations of this effect have been published in the literature. One of these calculations gives results that are qualitatively consistent with the data [13], while the other calculation [12] shows a much smaller effect. Neither of the two calculations includes full integration over the initial state kinematics and the medium density development. Another radiative scenario involves Cherenkov radiation of gluons [40, 41, 43], which would give rise to conical distributions.

Both for large-angle medium-induced gluon radiation and for gluon Cherenkov radiation, the expectation is that the away-side shape becomes narrower with increasing p_T^{assoc} [13, 41]. This trend is not observed in the correlation data: using a few different functional forms for the away-side distributions, we found that peak-separation Δ is approximately independent of p_T^{assoc} .

Alternatively, one could imagine that the passage of

high- p_T partons excites sound waves in the medium. It has been suggested that this may lead to Mach shock waves [14–17]. Qualitatively, the observed constant separation between the away-side peak and the constant conical emission angle from three-particle correlations [39] are consistent with this explanation. The transition from a broad away-side structure at low p_T to a narrow structure at higher p_T would then signal the change from away-side structures dominated by bulk particle production from the medium to a situation where jet-fragments dominate.

A recent 3D hydrodynamical calculation which includes local density fluctuations in the initial state also shows a broad away-side structure that may be consistent with the experimental di-hadron correlation data [29]. In this model, there is no explicit introduction of hard partons or jets; the correlation arises purely from the medium. At the moment, it is not clear whether this model will also generate the conical emission signal seen in three-particle correlation data [39]. A study of three-particle correlations in this model is ongoing [44].

In general, a number of different mechanisms, including fragmentation, radiative energy loss, bulk response and hadron formation by coalescence of constituent quarks, may contribute to the observed di-hadron correlation structures. Quantitative modeling of the different processes, including the azimuthal correlation of the trigger and associated hadrons with the reaction plane, is needed to further disentangle the observed signals and the background.

Experimentally, more insight in the underlying production processes will be gained from di-hadron measurements with identified particles and with respect to the reaction plane. In addition, γ -jet measurements, and measurements with reconstructed jets are being pursued, which provide better control over the initial state kinematics.

VI. ACKNOWLEDGEMENTS

We thank the RHIC Operations Group and RCF at BNL, the NERSC Center at LBNL and the Open Science Grid consortium for providing resources and support. This work was supported in part by the Offices of NP and HEP within the U.S. DOE Office of Science, the U.S. NSF, the Sloan Foundation, the DFG cluster of excellence ‘Origin and Structure of the Universe’ of Germany, CNRS/IN2P3, STFC and EPSRC of the United Kingdom, FAPESP CNPq of Brazil, Ministry of Ed. and Sci. of the Russian Federation, NNSFC, CAS, MoST, and MoE of China, GA and MSMT of the Czech Republic, FOM and NWO of the Netherlands, DAE, DST, and CSIR of India, Polish Ministry of Sci. and Higher Ed., Korea Research Foundation, Ministry of Sci., Ed. and Sports of the Rep. Of Croatia, Russian Ministry of Sci. and Tech, and RosAtom of Russia.

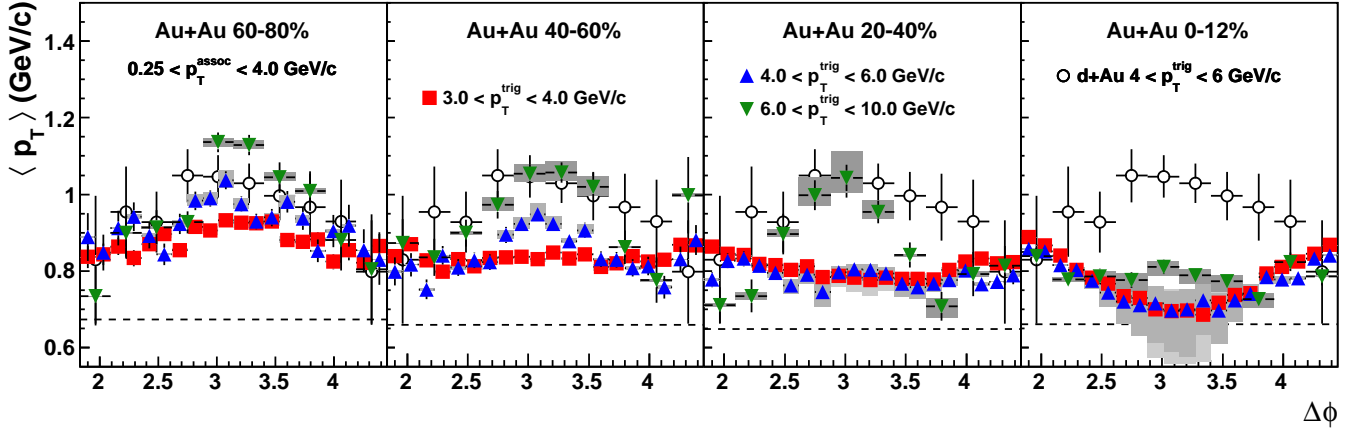


FIG. 8: (Color online) Mean transverse momentum $\langle p_T \rangle$ of associated particles with $0.25 < p_T^{assoc} < 4.0$ GeV/c, for four different centrality selections. The shaded bands show the systematic uncertainty due to elliptic flow of the uncorrelated background. The dashed lines indicate the inclusive $\langle p_T \rangle$ in the same p_T range in events with a trigger particle.

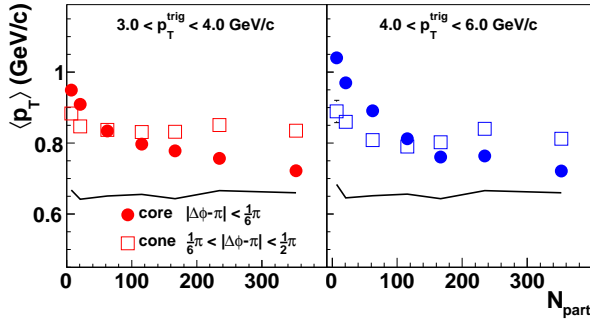


FIG. 9: (Color online) Mean transverse momentum $\langle p_T \rangle(\Delta\phi)$ of associated hadrons in the range $0.25 < p_T^{assoc} < 4.0$ GeV/c in the core ($|\Delta\phi - \pi| < \frac{\pi}{6}$) and cone ($\frac{\pi}{6} < |\Delta\phi - \pi| < \frac{\pi}{2}$) azimuthal regions for $3 < p_T^{trig} < 4$ GeV/c and $4 < p_T^{trig} < 6$ GeV/c as a function of number of participants. The lines indicate the inclusive $\langle p_T \rangle$ in the same p_T range for events with a trigger hadron.

-
- [1] J. Adams *et al.* (STAR), Phys. Rev. Lett., **91**, 072304 (2003), nucl-ex/0306024 .
- [2] M. Gyulassy and M. Plumer, Phys. Lett., **B243**, 432 (1990).
- [3] X.-N. Wang and M. Gyulassy, Phys. Rev. Lett., **68**, 1480 (1992).
- [4] R. Baier, Y. L. Dokshitzer, A. H. Mueller, S. Peigne, and D. Schiff, Nucl. Phys., **B483**, 291 (1997), hep-ph/9607355 .
- [5] C. Adler *et al.* (STAR), Phys. Rev. Lett., **89**, 202301 (2002), nucl-ex/0206011 .
- [6] K. Adcox *et al.* (PHENIX), Phys. Rev. Lett., **88**, 022301 (2001), nucl-ex/0109003 .
- [7] J. Adams *et al.* (STAR), Phys. Rev. Lett., **97**, 162301 (2006), nucl-ex/0604018 .
- [8] C. Loizides, Eur. Phys. J., **C49**, 339 (2007), hep-ph/0608133 .
- [9] H. Zhang, J. F. Owens, E. Wang, and X.-N. Wang, Phys. Rev. Lett., **98**, 212301 (2007), nucl-th/0701045 .
- [10] J. Adams *et al.* (STAR), Phys. Rev. Lett., **95**, 152301 (2005), nucl-ex/0501016 .
- [11] A. Adare *et al.* (PHENIX), Phys. Rev., **C78**, 014901 (2008), arXiv:0801.4545 [nucl-ex] .
- [12] I. Vitev, Phys. Lett., **B630**, 78 (2005), hep-ph/0501255 .
- [13] A. D. Polosa and C. A. Salgado, Phys. Rev., **C75**, 041901 (2007), hep-ph/0607295 .
- [14] H. Stoecker, Nucl. Phys., **A750**, 121 (2005), nucl-th/0406018 .
- [15] J. Casalderrey-Solana, E. V. Shuryak, and D. Teaney, J. Phys. Conf. Ser., **27**, 22 (2005), arXiv:hep-ph/0411315 .
- [16] T. Renk and J. Ruppert, Phys. Rev., **C73**, 011901 (2006),

- hep-ph/0509036 .
- [17] J. Ruppert and B. Muller, Phys. Lett., **B618**, 123 (2005), arXiv:hep-ph/0503158 .
- [18] R. C. Hwa and C. B. Yang, Phys. Rev., **C66**, 025205 (2002), hep-ph/0204289 .
- [19] R. J. Fries, B. Muller, C. Nonaka, and S. A. Bass, Phys. Rev. Lett., **90**, 202303 (2003), nucl-th/0301087 .
- [20] V. Greco, C. M. Ko, and P. Levai, Phys. Rev. Lett., **90**, 202302 (2003), arXiv:nucl-th/0301093 .
- [21] K. H. Ackermann *et al.* (STAR), Nucl. Instrum. Meth., **A499**, 624 (2003).
- [22] M. Anderson *et al.*, Nucl. Instr. Meth., **A499**, 659 (2003).
- [23] F. S. Bieser *et al.* (STAR), Nucl. Instrum. Meth., **A499**, 766 (2003).
- [24] J. Adams *et al.* (STAR), Phys. Rev., **C72**, 014904 (2005), nucl-ex/0409033 .
- [25] N. N. Ajitanand *et al.*, Phys. Rev., **C72**, 011902 (2005), arXiv:nucl-ex/0501025 .
- [26] J. Adams *et al.* (Star), Phys. Rev., **C75**, 034901 (2007), nucl-ex/0607003 .
- [27] T. A. Trainor, Phys. Rev., **C81**, 014905 (2010), arXiv:0904.1733 [hep-ph] .
- [28] S. A. Voloshin, Phys. Lett., **B632**, 490 (2006), arXiv:nucl-th/0312065 .
- [29] J. Takahashi *et al.*, Phys. Rev. Lett., **103**, 242301 (2009), arXiv:0902.4870 [nucl-th] .
- [30] J. Liao and E. Shuryak, Phys. Rev., **C77**, 064905 (2008), arXiv:0706.4465 [hep-ph] .
- [31] A. Dumitru, F. Gelis, L. McLerran, and R. Venugopalan, Nucl. Phys., **A810**, 91 (2008), arXiv:0804.3858 [hep-ph] .
- [32] S. Gavin, L. McLerran, and G. Moschelli, Phys. Rev., **C79**, 051902 (2009), arXiv:0806.4718 [nucl-th] .
- [33] J. Adams *et al.* (STAR), Phys. Rev., **C73**, 064907 (2006), nucl-ex/0411003 .
- [34] B. I. Abelev *et al.* (STAR), Phys. Rev., **C80**, 064912 (2009), arXiv:0909.0191 [nucl-ex] .
- [35] R. C. Hwa and C. B. Yang, Phys. Rev., **C70**, 024905 (2004), arXiv:nucl-th/0401001 .
- [36] C. B. Chiu and R. C. Hwa, Phys. Rev., **C72**, 034903 (2005), arXiv:nucl-th/0505014 .
- [37] A. Adare *et al.* (PHENIX), Phys. Lett., **B649**, 359 (2007), arXiv:nucl-ex/0611016 .
- [38] S. S. Adler *et al.* (PHENIX), Phys. Rev., **C71**, 051902 (2005), arXiv:nucl-ex/0408007 .
- [39] B. I. Abelev *et al.* (STAR), Phys. Rev. Lett., **102**, 052302 (2009), arXiv:0805.0622 [nucl-ex] .
- [40] A. Majumder and X.-N. Wang, Phys. Rev., **C73**, 051901 (2006), nucl-th/0507062 .
- [41] V. Koch, A. Majumder, and X.-N. Wang, Phys. Rev. Lett., **96**, 172302 (2006), nucl-th/0507063 .
- [42] S. Zhang, G. L. Ma, Y. G. Ma, X. Z. Cai, J. H. Chen, H. Z. Huang, W. Q. Shen, X. H. Shi, F. Jin, J. Tian, C. Zhong, and J. X. Zuo, Phys. Rev. C, **76**, 014904 (2007).
- [43] I. M. Dremin, JETP Lett., **30**, 140 (1979).
- [44] R. Andrade, F. Grassi, Y. Hama, and W. L. Qian, (2009), arXiv:arXiv:0912.0703 [nucl-th] .

Appendix: Background shapes

In this Appendix, we show the associated hadron azimuthal distributions before subtracting the flow background.

Figure 10 shows the distributions for associated particles between 1.0 and 2.5 GeV/ c and for different ranges of trigger particle p_T , ranging from 2.5 – 3.0 GeV/ c (left column) to 6 – 10 GeV/ c (right column) and different centralities (rows). Note the large increase of the combinatorial background with centrality. A large background modulation due to elliptic flow is expected.

Figure 11 shows the distributions of associated charged particles with various p_T^{assoc} and p_T^{trig} selections for 0–12% central Au+Au collisions. For $p_T^{assoc} > 1.0$ GeV/ c (lower three rows), the value of $1/N_{trig}dN/d\Delta\phi$ at the minimum depends mostly on p_T^{assoc} , as expected for uncorrelated background. In the upper row however, with $0.5 < p_T^{assoc} < 1.0$ GeV/ c , we observe a significant dependence of $1/N_{trig}dN/d\Delta\phi$ at the minimum on p_T^{trig} . The value at the minimum increases for lower p_T^{trig} , which is qualitatively consistent with a centrality bias combined with the fact that the probability to find more than one trigger particle per event is sizable for the lower p_T^{trig} selections and decreases with increasing p_T^{trig} .

The background normalization (B) and the elliptic flow $\langle v_2^{assoc} \rangle \langle v_2^{trig} \rangle$ that were used to subtract the background in Figs 2 and 3 are reported in Tables I and II.

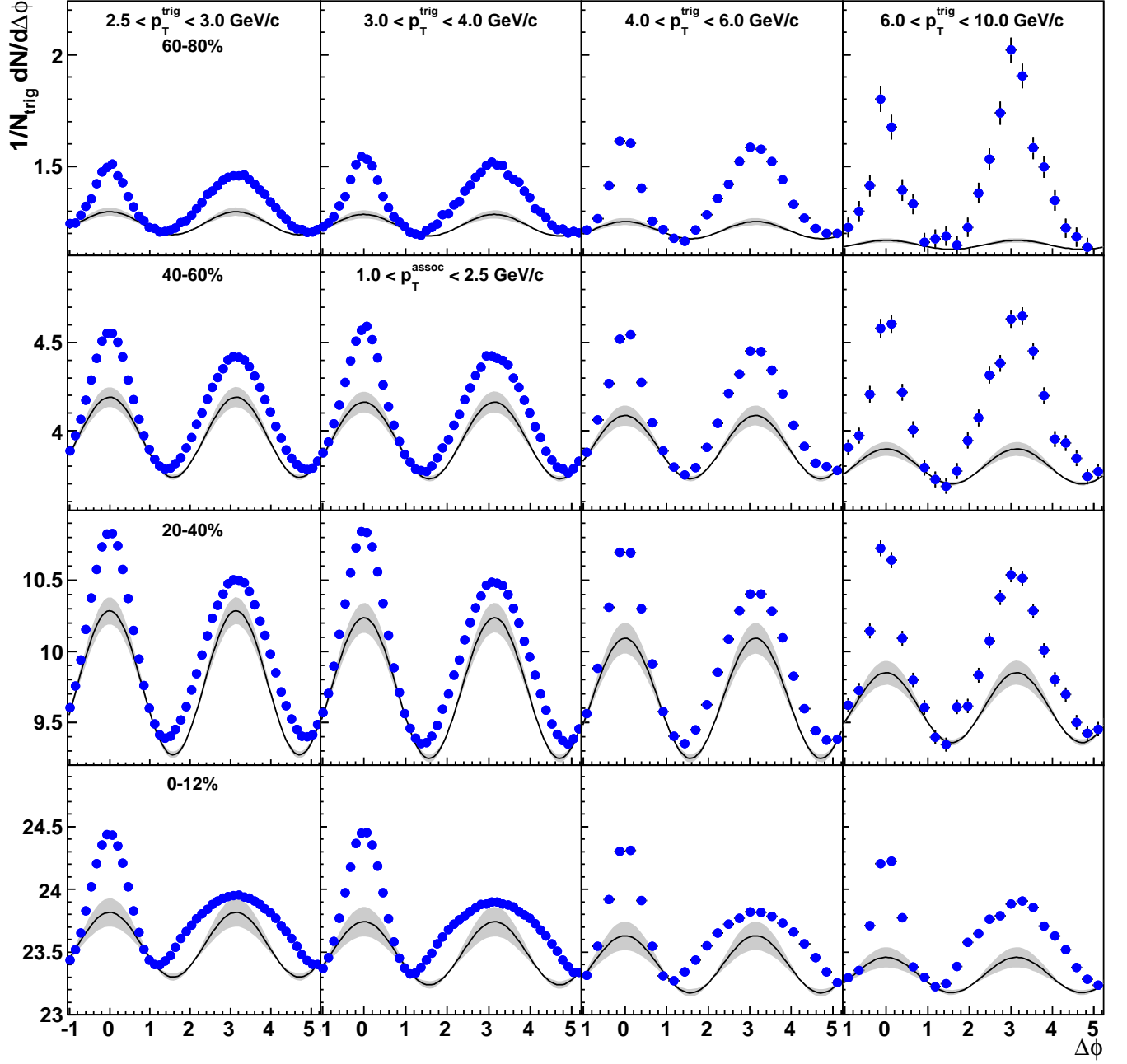


FIG. 10: (Color online) Azimuthal angle difference distributions for associated particles with p_T between 1.0 and 2.5 GeV/c and for different ranges of trigger particle p_T , ranging from 2.5 – 3.0 GeV/c (left column) to 6 – 10 GeV/c (right column). Results are shown for Au+Au collisions with different centrality (rows). The line and the grey band show the elliptic flow modulated background that was subtracted to obtain Fig. 2.

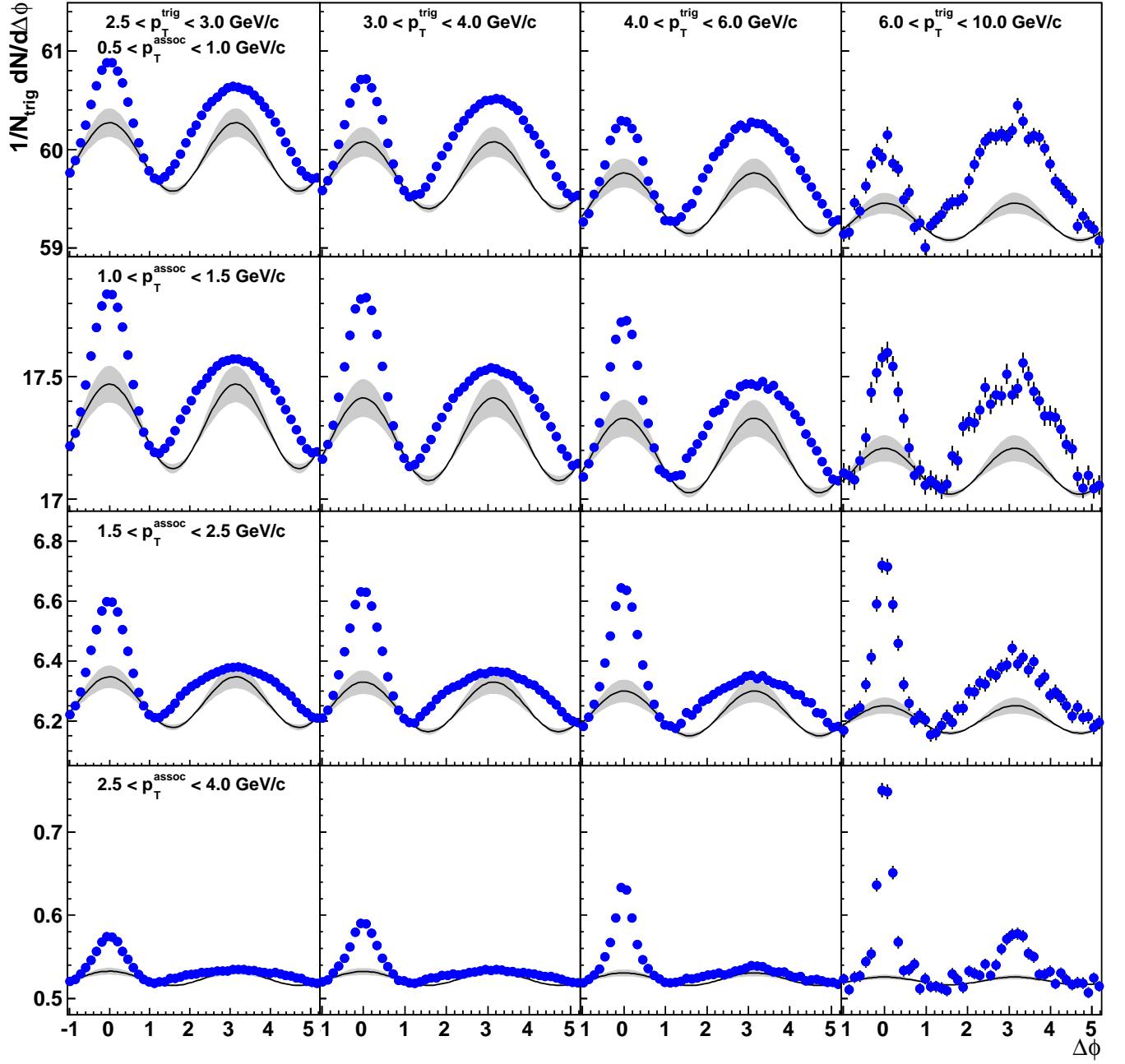


FIG. 11: (Color online) Azimuthal angle difference distributions for different p_T^{trig} (columns) and p_T^{assoc} (rows) in 0-12% central Au+Au collisions. The line and the grey band show the elliptic flow modulated background that was subtracted to obtain Fig. 3.

p_T^{trig} (GeV/c)	$B_{ \Delta\eta <2.0}$	$\langle v_2^{assoc} \rangle \langle v_2^{trig} \rangle$ (10^{-3})
60-80%		
2.5 - 3.0	1.220 ± 0.002	20.6 ± 4.6
3.0 - 4.0	1.214 ± 0.003	19.4 ± 4.6
4.0 - 6.0	1.197 ± 0.008	15.7 ± 4.1
6.0 - 10.0	1.139 ± 0.026	8.67 ± 2.7
40-60%		
2.5 - 3.0	3.846 ± 0.002	28.6 ± 4.4
3.0 - 4.0	3.835 ± 0.003	27.5 ± 4.6
4.0 - 6.0	3.820 ± 0.008	22.9 ± 4.5
6.0 - 10.0	3.76 ± 0.03	13.0 ± 3.2
20-40%		
2.5 - 3.0	9.522 ± 0.002	25.9 ± 3.0
3.0 - 4.0	9.494 ± 0.003	25.4 ± 3.3
4.0 - 6.0	9.466 ± 0.008	21.8 ± 3.4
6.0 - 10.0	9.515 ± 0.031	12.8 ± 2.7
0-12%		
2.5 - 3.0	23.531 ± 0.001	5.5 ± 1.5
3.0 - 4.0	23.469 ± 0.002	5.4 ± 1.6
4.0 - 6.0	23.395 ± 0.005	4.9 ± 1.5
6.0 - 10.0	23.365 ± 0.021	3.0 ± 1.1

TABLE I: The v_2 and the normalization values used for the background subtraction in Fig. 2.

p_T^{trig} (GeV/c)	$B_{ \Delta\eta <2.0}$	$\langle v_2^{assoc} \rangle \langle v_2^{trig} \rangle$ (10^{-3})
$0.5 < p_T^{assoc} < 1.0$ GeV/c		
2.5 - 3.0	59.833 ± 0.002	2.9 ± 0.8
3.0 - 4.0	59.638 ± 0.003	2.8 ± 0.8
4.0 - 6.0	59.366 ± 0.009	2.6 ± 0.8
6.0 - 10.0	59.235 ± 0.034	1.6 ± 0.6
$1.0 < p_T^{assoc} < 1.5$ GeV/c		
2.5 - 3.0	17.286 ± 0.001	5.0 ± 0.1
3.0 - 4.0	17.238 ± 0.002	4.9 ± 0.1
4.0 - 6.0	17.182 ± 0.005	4.4 ± 0.1
6.0 - 10.0	17.154 ± 0.018	2.7 ± 0.1
$1.5 < p_T^{assoc} < 2.5$ GeV/c		
2.5 - 3.0	6.245 ± 0.001	6.8 ± 1.9
3.0 - 4.0	6.230 ± 0.001	6.6 ± 2.0
4.0 - 6.0	6.213 ± 0.003	6.0 ± 1.9
6.0 - 10.0	6.211 ± 0.011	3.7 ± 1.4
$2.5 < p_T^{assoc} < 4.0$ GeV/c		
2.5 - 3.0	0.5210 ± 0.0002	8.1 ± 2.4
3.0 - 4.0	0.5212 ± 0.0003	8.0 ± 2.5
4.0 - 6.0	0.5207 ± 0.0008	7.2 ± 2.4
6.0 - 10.0	0.5199 ± 0.0030	4.5 ± 1.7

TABLE II: The v_2 values and the normalization used for the background subtraction in Fig. 3.

